Characterization of Amphiphilic Diblock Copolymers Synthesized by MADIX Polymerization Process

Marc Jacquin, Pierre Muller, Gilda Lizarraga, Corinne Bauer, Hervé Cottet, Olivier Théodoly

Characterization of Amphiphilic Diblock Copolymers Synthesized by MADIX Polymerization Process

Marc Jacquin,[†] Pierre Muller,[†,||] Gilda Lizarraga,[‡] Corinne Bauer,[‡] Hervé Cottet,[§] and Olivier Théodoly*,[†,⊥]

Complex Fluids Laboratory, CNRS UMR 166, 350 George Patterson Blvd, Bristol Pennsylvania 19007, and Rhodia CRTB, 350 George Patterson Blvd, Bristol Pennsylvania 19007, and Equipe Dynamique des Systèmes Biomoléculaires Complexes, CNRS UMR 5073, Université de Montpellier 2, place Eugène Bataillon CC 017, 34095 Montpellier Cedex 5, France, and Institut Charles Sadron, 6 rue Boussingault, 67083 Strasbourg Cedex, France, and Laboratoire Adhésion et Inflammation, INSERM U600, CNRS UMR 6212, Case 937, 163 Avenue de Luminy, Marseille F-13009, France, and Faculté des Sciences/de Médecine ou de Pharmacie, Aix-Marseille Université Marseille, F-13000, France

ABSTRACT: We combined several analytical techniques (NMR, matrix assisted laser desorption ionization -time-of-flight mass spectroscopy MALDI−TOF MS, GPC, functional analysis on the first block, liquid chromatography at the point of exclusion adsorption transition LC-PEAT, and capillary electrophoresis CE) to analyze and quantify the characteristics of homopolymer precursors and amphiphilic diblocks synthesized by controlled radical polymerization process (CRP). We present here a detailed quantitative characterization of amphiphilic diblock copolymers (poly(butyl acrylate)−poly(acrylic acid) or PBA-*b*-PAA, and poly(di(ethylene glycol) ethyl ether acrylate)−poly(acrylic acid) or PDEGA-*b*-PAA). The samples were synthesized in ethanol by macromolecular design via inter-exchange of xanthate (MADIX), a reversible addition fragmentation transfer (RAFT) polymerization process using xanthates as control agents. The analytical results have permitted a determination of the transfer constant of xanthate C_{Xa} ($\approx$ 2.7 and 1.5 for respectively PBA and PDEGA) and the transfer constant to solvent C_s ($\approx 6 \times 10^{-4}$). In the final diblock products, homopolymer side products were characterized. The amount of hydrophobic homopolymer was quantified by a specially developed LCPEAT technique in critical conditions for PBA. The hydrophilic homopolymer *h*-PAA amount was determined by quantitative capillary electrophoresis CE experiments. These analytical approaches allowed the quantification of the side products in a CRP system as well as the improvement of the reaction conditions via a thorough knowledge of the reaction mechanism.

1. Introduction

Synthesis of polymer chains with complex architectures is an important and challenging activity in the industry of specialty chemicals. The goal is to engineer new components with targeted physical properties. Over the past decade, various controlled radical polymerization (CRP) techniques like atom transfer radical polymerization (ATRP), stable-free radical polymerization (SFRP), reversible addition fragmentation transfer (RAFT), or macromolecular design via inter-exchange of xanthate (MADIX) have emerged as new routes to design complex molecules with a high variety of chemical compounds and at reasonable production costs. These techniques permit, for instance, the synthesis of block copolymers, graft polymers, gradient polymers, star polymers, and microgels. The polymerization processes (in bulk, solution, or emulsion), the choice of control agents (nature of leaving and stabilizing group),[1−3] and experimental conditions (temperature, time, amount of initiator) have been optimized for the synthesis of many components. CRP processes allow polymerization of a large variety of chemistries, like monomers of acrylate, methacrylate, vinyl, and styrene derivatives. This is a noticeable advantage over the anionic processes which are limited to a few monomers (butadiene, styrene, isoprene, *tert*-butyl acrylate, methyl methacrylate propylene oxide, and ethylene oxide).

Besides all the advantages of CRP techniques, one drawback is that CRP syntheses lead to side products and nonnegligible polydispersities. Few works in the literature have attempted to characterize homopolymers synthesized by CRP. However, the few studies that have looked at this problem carefully have shown the importance of side reactions.[4−6] CRP techniques are based on the growth of radical chains, so that transfer or termination events during the process are sources of side products. Routine analysis by gel permeation chromatography GPC and NMR does not provide enough insight in order to detect and characterize the nature and amount of these side products. Taking the simple case of a homopolymer synthesis, CRP leads to a typical index of polydispersity I_p between 1.2 and 2. Although such values represent a great improvement as compared to the ones obtained via uncontrolled radical polymerization (around 3), polydispersities of CRP samples are not negligible. Taking now the case of block copolymers, a characteristic shift in the mass distribution detected by GPC before and after the growth of the second block does not prove that all monomers have grown on the precursors. Homopolymers, branched polymers and multiblocks may also have been produced and specific analysis techniques are required to recognize between all these species. Therefore, the control of CRP product characteristics requires a precise knowledge of

* Corresponding author.
† Complex Fluids Laboratory, CNRS UMR 166.
‡ Rhodia CRTB.
§ Equipe Dynamique des Systèmes Biomoléculaires Complexes, CNRS UMR 5073, Université de Montpellier 2.
|| Institut Charles Sadron.
⊥ Laboratoire Adhésion et Inflammation, INSERM U600, CNRS UMR 6212, and Faculté des Sciences/de Médecine ou de Pharmacie, Aix-Marseille Université.

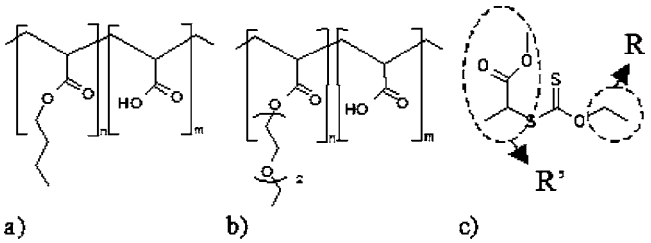

Figure 1. Structures of (a) poly(butyl acrylate)-*b*-poly(acrylic acid), (b) poly(diethylene glycol ethyl ether)-*b*-poly(acrylic acid), and (c) Rhodixan A1.

the reaction mechanism. In order to identify this mechanism, a precise analysis of products and side products for each reaction step is necessary.

So far, the characterization and the quantification of side-products generated during CRP processes have attracted little attention.[4−6] The present work proposes an in depth analysis of an amphiphilic diblock copolymer sample of poly(butyl acrylate)−poly(acrylic acid) or PBA-*b*-PAA (Figure 1a) synthesized by a CRP technique (MADIX process[7−9]). The synthesis of PBA-*b*-PAA has already been reported by several polymerization processes. Lefay et al.[10] reported the synthesis of PBA-*b*-PAA using nitroxide mediated free radical polymerization in dioxane at 120 °C. Couvreur et al.[11] performed homopolymer PAA synthesis in similar conditions and showed that the polymerization was controlled ($I_p \approx 1.4$), but that transfer to solvent generated dead chains especially for high targeted molar masses ($M_n > 40\,000$ g/mol). The latter effect was also responsible for an increase of the polydispersity from 1.4 to 1.8. Polymerization of a second block of PBA grown on the PAA precursor led to a poor final polydispersity index of 3.3. More successful results were obtained by Chong et al.[12] for syntheses of PBA-*b*-PAA samples by RAFT in DMF. They obtained block copolymers with final polydispersity indexes of 1.2. The drawback of this protocol is its inconvenience for industrial scale-up because of the low conversion of monomers and of the difficult removal of DMF, which is a toxic solvent. Gaillard et al.[13] reported the synthesis of PBA-*b*-PAA diblock copolymers by RAFT in ethanol, based on previous work on PAA synthesis in protic media.[6,14] This route for PBA-*b*-PAA synthesis seemed realistic for industrial production. In this work, a MADIX process, which is similar to RAFT, has been used. It is characterized by the use of a xanthate as a stabilizing agent. The MADIX process for PBA-*b*-PAA has already been successfully scaled-up for industrial production by Rhodia. Finally, as this short overview of CRP synthesis of PBA-*b*-PAA shows, the obtention of a good product is not straightforward, and no quantitative analysis of side products has been performed.

We present in this paper a thorough analysis of MADIX produced PBA-*b*-PAA samples, which allowed us to clarify the mechanism of the MADIX process and to improve the synthesis protocol. We have combined numerous analytical techniques. LC−PEAT adapted to PBA was specially developed for this study. We first focus on the analysis of homopolymers, which were produced in the first step of the diblocks synthesis. For homopolymers *h*-PBA samples, the populations of both stabilized and dead chains have been characterized by GPC using functional analysis. We then present the analysis of diblocks PBA-*b*-PAA, synthesized by the growth of a PAA block on the *h*-PBA precursor. LC−PEAT and capillary electrophoresis performed on the final products were used to estimate the amount of dead chains of the first and second blocks. In order to point out the robustness (and eventual limitations) of this analysis protocol, it has been applied to another family of amphiphilic diblocks, the poly(di(ethylene glycol) ethyl ether acrylate)−poly(acrylic acid) or PDEGA-*b*-PAA (Figure 1b). PDEGA-*b*-PAA is a class of block copolymers newly developed for optimum surface active properties. It differs from the PBA-*b*-PAA only by the chemical nature of the hydrophobic block.

2. Experimental Section

Materials. We used Rhodixan A1 (2-mercaptopropionic acid, methyl ester, *o*-ethyl dithiocarbonate (Figure 1c)) provided by Rhodia (99% NMR purity) as a control agent. Rhodixan A1 has already proven to be efficient for the controlled polymerization of a broad range of monomers.[15]

Monomers of acrylic acid (AA, Aldrich, 147230, 99%), butyl acrylate (BA, Aldrich, 234923, 99%) and butyl-d_9 acrylate (Polymer Source, D9nBUA, 98%) were used as received. Di(ethylene glycol) ethyl ether acrylate monomers (DEGA, Aldrich, 408298, 90%) were technical grade, which was the highest purity commercially available. GC−MS analysis on DEGA monomers allowed us to detect two minor impurities (<5% each) with molecule fragments identical to those of the major product. ^{1}H NMR indicated an excess of ethylene oxide groups as compared to the theoretical formula. The conclusion is that the two impurities are monomers with longer ethylene oxide pendent chains.

Two initiators were used, 2,2′-azobis(2-methylbutanenitrile) (DuPont, AMBN Vazo 67, 98%) and *tert*-butyl peroxypivalate (AkzoNobel, Trigonox 25-C75, 75% solution in mineral spirits). All solvents and gases were analytical grade. Water was purified using a Milli-Q plus water purification system.

Polymerization. Typical polymerization reactions were performed at a concentration of 40 wt % in ethanol for each block. We used either a 500 mL kettle reactor or a high-throughout set up (ASW 2000, ChemSpeed coupled with a GPC in-line) with 12 100 mL reactors. In both cases, reactors were equipped with a cold water condenser. Jacketed reactors were brought to 70 °C, and sparged with nitrogen for half an hour. A shot of initiator was added for the growth of each block. The initiator amount was equal to one tenth of the xanthate amount in moles. The xanthate amount was adapted according to the targeted molar mass M_t by eq 1

$$M_t = M_0 \frac{n_M}{n_{Xa}} \tag{1}$$

where M_0 is the molar mass of the monomer and n_M and n_{Xa} are the number of moles of monomer and xanthate in the reactor. Typical reaction time was 8 to 12 h for each block to achieve 99% conversion. For instance, a PBA-*b*-PAA of 3K−12K was prepared by dissolving 32.09 g (0.2503 mol) of butyl acrylate and 2.22 g (1.065×10^{-2} mol) of xanthate in 38.04 g (0.8257 mol) of ethanol in a 500 mL reactor. The mixture was brought to 70 °C and sparged with N_2 for half an hour. We then added 0.371 g (2.197×10^{-3} mol) of initiator Trigonox by addition of 0.494 g of a Trigonox 25-C75 solution diluted in 10.00 g of ethanol (0.2170 mol) at a flow rate of 1 mL/h. After 12 h, the percent solid was measured at 44%. We took 16.82 g of the product for chemical analysis of first block. The temperature of the reactor was then set to 65 °C to avoid overheating upon addition of acrylic acid. We added 100.19 g (1.3903 mol) of acrylic acid, 140.15 g (3.042 mol) of ethanol and sparged with N_2 for half an hour. We then added 0.287 g (1.647×10^{-3} mol) of initiator Trigonox by addition of 0.323 g of a Trigonox 25-C75 solution diluted in 10.14 g (0.2201 mol) of ethanol at a flow rate of 1 mL/h. After 1 h, the temperature was set to 70 °C for another 11 h. The final percent solid was measured at 40%. All chemical analysis results of the first block *h*-PBA and diblock PBA-*b*-PAA 3K−12K are presented in the following.

Conversion Determination. The global conversion rate was followed by percent solids measurements using a moisture balance Mettler PM 480/LP 16.

The conversion rate of controlling agent Rhodixan A1 and monomers BA and DEGA has been measured with a HPLC system (Agilent 1100 series) using UV detection at 210 nm. The HPLC

column was a SUPELCOSIL LC-18 (250 × 4.6 mm, 5 μm) with a mobile phase methanol/water 75/25 v/v and a flow rate of 1 mL/min. Precise determinations of residual monomers were obtained with a Hewlett-Packard GC 5890 device equipped with head space sampler 7694 and a FID detection system. The GC column was a ZorBax-1 (60 m × 0.53 mm) with a flow of helium of 1 mL/min. The temperature of the sample was fixed at 105 °C. The temperature of the oven was put at 60 °C for 5 min, then increased with a ramp of 15 °C/min, and kept at 250 °C for 5 min more.

NMR. ^{1}H 400 MHz and ^{13}C 100 MHz NMR spectra were measured using a Varian Unity Inova 400. ^{1}H NMR spectroscopy was performed either in D_2O or in $CDCl_3$. ^{13}C NMR was performed in DMSO in presence of chromium acetyl acetonate to decrease the relaxation times of carbons and allow quantitative analysis from ^{13}C NMR data.

MALDI-TOF MS. Matrix assisted laser desorption ionization−time-of-flight mass spectroscopy MALDI-TOF MS spectra were recorded on a BIFLEX III (Bruker) apparatus. This instrument, equipped with a nitrogen laser (337 nm) and delayed extraction, was operated at an accelerating potential of 20 kV in linear mode. The MALDI mass spectra represent averages over 100 consecutive laser shots (1 Hz repetition rate). Polymer samples were dissolved at a concentration of 6 mg/mL in a 90/10 ethanol/water solution at 0.01 M NaCl. The matrix used was a 10 mg/mL (4-(4-nitrophenylazo)resorcinol). Internal standards (ethoxylated nonylphenol) were used to calibrate the mass scale using calibration software from Biflex III.

Molar Mass Determination. Molar mass distributions of hydrophobic polymers were determined by GPC (Agilent 1100 series). A pump, an auto-sampler, a refractive index detector and a UV detector at 290 nm were mounted in series. A set of three Columns from Polymer Laboratories PLgel Mixed-B (particle size 8−10 μm, range of MW 500−10 000 000 g/mol) were used in series with THF as a mobile phase at a temperature of 40 °C and a flow rate of 0.75 mL/min. Polystyrene standards (Polymer Laboratories EasiCal PS-2) were used for calibration. We used the principle of universal calibration[16] to adapt the PS based calibration to PBA samples. For each elution time, the product of the intrinsic viscosity [η] and the molar mass M is a constant for any polymer. Using the Mark−Houwink expression of the intrinsic viscosity [η], one can write for any chain of mass M_i:

$$KM_i^{1+a} = K_{PS}M_{PS}^{1+a_{PS}} \quad (2)$$

where K, K_{PS}, and a and a_{PS} are the Mark−Houwink coefficients for h-PBA and h-PS. Mark−Houwink coefficients were taken from literature[17] data, $K = 1.22 \times 10^{-4}$ dL/g and $a = 0.700$ for PBA, and $K_{PS} = 1.14 \times 10^{-4}$ dL/g and $a_{PS} = 0.716$ for PS.

PBA-*b*-PAA samples were methylated prior to GPC analysis in order to suppress interactions between PAA and the stationary phase. Methylation was performed by first dissolving the diblock samples in DMF with 2 equiv of iodomethane relative to acrylic acid groups. One equivalent of tetrabutyl ammonium hydroxide was then slowly added from a methanol solution over a period of 4 h. The reaction was run for 48 h in the dark. The reaction yield, determined by ^{13}C NMR spectroscopy in $CHCl_3$, showed that over 90% of acrylic acid groups were methylated. Prior to injection in GPC, the methylated polymer was precipitated in water and dialyzed vs pure water in 2000 MWCO dialysis bags in order to eliminate residual salt of tetrabutyl ammonium iodide. We used PS calibration for the GPC of methylated diblocks.

LC-PEAT. Liquid chromatography at the point of exclusion and adsorption transition is particularly adapted to block copolymer analysis.[18−23] In the exclusion regime, polymers have no interaction with the stationary phase. Low molar mass polymers penetrate in the pores of the stationary phase, whereas high molar mass polymers are excluded from it. The higher the molar mass is, the lower the elution time. In the adsorption regime, polymers have interactions with the stationary phase, so that the retention times increase with the molar mass. In conditions where the effects of exclusion and adsorption are exactly balanced, i.e., in the so-called critical conditions, polymer chains are eluted with no dependence on their molar mass. Consequently, in critical conditions, elution time is only sensitive to changes of the chemical composition of chains. This property is suited for separation of homopolymers and diblocks. In the case of h-PBA homopolymers, the critical conditions have been precisely determined with samples of MW 1K, 3K, 30K, 60K, 80K, 100K, and 120K at room temperature, i.e., 21−25 °C, on a stationary phase Zorbax SB C_{18} (250 × 4.6 mm, 300 Å) with a mobile phase made of a THF/H_2O mixture of volume ratio comprised between (90/10) (v/v) and (89/11) (v/v). PEAT conditions were determined for each column and before each series of experiments. The history of the column proved to be a very important factor with great influence on the eluent composition at the PEAT. The eluent composition at PEAT changed in the range of one % depending on the column history. At PEAT, the temperature was not controlled but variations of ±2 °C have not proven to have a dramatic effect on the PEAT. Measurements have been performed on a Waters HPLC, auto-sampler 717 plus and pump 515. The flow rate was set to 1 mL/min. Typically, 10 μL of a 1 wt % solution degassed under He for half an hour were injected. Detection used an evaporative light scattering detector (ELSD) SEDERE PL EMD-960 regulated at 40 °C, with a gas flow of 3.5-5 mL/min. Detector response was calibrated by injections of known amounts of homopolymer h-PBA. In order to determine the h-PBA homopolymer content, ELSD detector was calibrated using a h-PBA 3K sample in the mobile phase at different known concentrations. It was checked that the calibration does not depend on the M_w of the h-PBA used for calibration.

Capillary Electrophoresis. CE is an analytical separation technique based on the differential migration of ionic species under electric field.[24,25] Separation occurs in a narrow bore capillary (25−200 μm diameter) using very high electric field. In capillary zone electrophoresis (CZE), the capillary is filled with a buffer and both ends of the capillary are dipped in reservoirs filled with the same buffer. Samples are injected in the capillary, whereas buffer conditions and electric field are kept constant. The apparent electrophoretic mobility μ_{app} of the solute is defined according to eq 3:

$$\mu_{app} = \frac{v_{app}}{E} = \frac{Ll}{Vt_{app}} \quad (3)$$

where v_{app} is the apparent electrophoretic velocity, E is the electric field, L the length of the capillary, l the migration length, V the applied voltage, and t_{app} the apparent migration time of the solute. The apparent mobility is the sum of two contributions. One is directly due to the effective electrophoretic mobility of the solute, μ_{ep}, relative to the aqueous phase. The other is due the mobility of the solvent as an electroosmotic flow is induced by the electric field in the capillary. Indeed, under basic conditions (typically pH around 9 in our experiments), the wall of the fused silica is negatively charged. An electroosmotic flow is generated by an electric field that flows toward the cathode. Our polymers are negatively charged and migrate in counter-electroosmotic mode (i.e., against the electroosmotic flow). The effective electrophoretic mobility μ_{ep} is related to the apparent electroosmotic mobilities μ_{app} according to eq 4:

$$\mu_{ep} = \mu_{app} - \mu_{eo} = \frac{Ll}{Vt_{app}} - \frac{Ll}{Vt_{eo}} \quad (4)$$

where μ_{eo} is the electroosmotic mobility, t_{eo} is the migration time of a neutral molecule, and mobilities have algebraic values (cations have positive μ_{ep} while anions have negative μ_{ep} values).

Micellar electrokinetic chromatography[26−28] (MEKC) is a particular type of CZE. In MEKC, surfactant is added in the electrolyte buffer. The Electroosmotic flow is marginally affected. The apparent mobility of a molecule may however be significantly modified if this molecule interacts with the surfactant. This is the case for amphiphilic diblocks and MCKE is very helpful as a complement to CZE in order to identify peaks in an electropherogram.

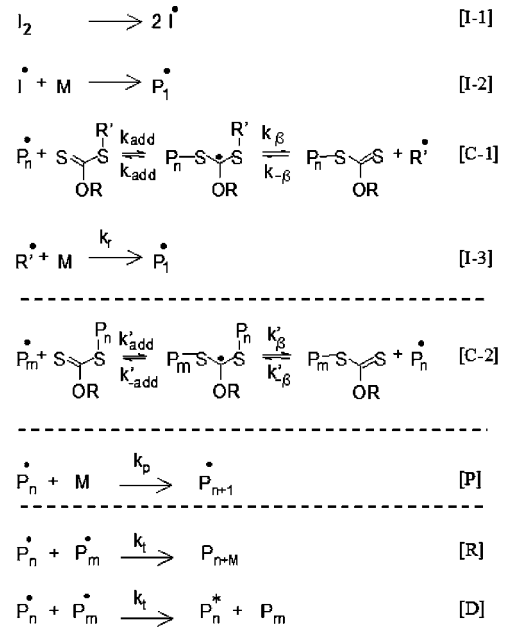

Figure 2. Macromolecular design via inter-exchange of xanthate MADIX polymerization mechanism. (●) indicates a radical and (∗) indicates an unsaturation.

All CE experiments were performed on an Agilent technologies capillary electrophoresis system, UV detection is used at 200 and 290 nm to detect respectively acrylate groups and both acrylate groups and xanthate groups. Capillaries were prepared from bare silica tubing purchased from Composite Metal Services (Worcester, United Kingdom). Capillary dimensions were $L = 33.5$ cm ($l =$ 25 cm to the detector) × o.d. 50 μm. Buffer used is a sodium borate buffer 160 mM fixing the pH at 9.2. Capillaries were first conditioned with the following flushes: 1 M NaOH for 15 min, 0.1 M NaOH for 10 min. Between injections, capillaries surfaces were regenerated using the following procedure: 5 min flush of 1 M NaOH, 2 min flush of 0.1 M NaOH, application of a potential V of +1 kV in 0.1 M NaOH, 5 min flush of the buffer. Samples at 1 wt % in the buffer were introduced hydrodynamically (∼4 μL) by application of a positive pressure on the inlet side of the capillaries (17−40 mbar for 3 s). Mesityl oxide (∼0.1% (v/v) in the borate buffer) was co-injected with the sample to determine the electroosmotic mobility. The applied potential V was +16 kV. The temperature of the capillary cartridge was set to 25 °C.

For relative quantification of the components appearing in different peaks in the electropherograms, the integration of the peaks is calculated vs the effective electrophoretic mobility. In presence of added surfactants, the effect induced by the slight change of the electrolyte viscosity were corrected according to eq 5, where the tracer acrylic acid is used as reference:

$$\mu_{ep}^{ion} = \frac{{}^{*}\mu_{ep}^{ion}}{{}^{*}\mu_{ep}^{tracer}} \mu_{ep}^{tracer} \tag{5}$$

where the asterisk marks the mobilities observed in the presence of surfactants.

3. Results and Discussion

Before entering the result section, we present the basics of MADIX mechanism that will guide our analysis protocol and discussion. The mechanism reactions are sketched in Figure 2. The initiation steps ([I-1] and [I-2]), the propagation step [P], and the termination steps (recombination [R] and disproportionation [D]) are the same as for uncontrolled radical polymerizations. The key of control comes from the stabilizing agent xanthate. There are two competing reversible transfer exchange reactions.

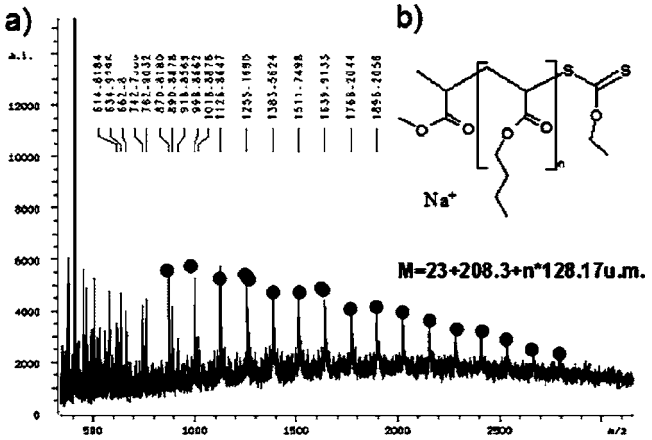

Figure 3. (a) Matrix assisted laser desorption ionization−time-of-flight mass spectroscopy MALDI−TOF MS spectrum of a homopolymer poly(butyl acrylate) *h*-PBA 1500 g/mol. The peaks marked by (●) correspond to molecules of the chemical structure of b.

Reaction [C-1] in Figure 2 corresponds to the transfer of the growing radical $P_n^{\bullet}$ on the xanthate R′−Xa. This creates a dormant chain P_n−Xa and a radical R′$^{\bullet}$ that can initiate another chain according to step [I-3]. The second transfer exchange is reaction [C-2] in Figure 2. It corresponds to the exchange of the xanthate group from a dormant chain P_n-Xa to a growing chain $P_n^{\bullet}$.

A. Homopolymers *h*-PBA—Xa and *h*-PDEGA—Xa.

MALDI—TOF MS: Evidence of Transfer Reactions. Experimental data obtained for *h*-PBA oligomers of mass 1000 g/mol are presented in Figure 3a. It displays a series of peaks regularly separated by a gap of 128 mass units, that matches the molar mass of a monomer BA. The peaks correspond therefore to chains of *h*-PBA with different degrees of polymerization. A closer look at the absolute values shows that the peaks correspond to the chemical structure of Figure 3b, i.e., *h*-PBA chains started by the labile part of the xanthate (reaction I-3) and ended by the stabilizing part of the xanthate (reaction C-1 and/or C-2). This is a good indication that most chains are initiated by xanthate and stabilized by xanthate, which is the basis of controlled radical polymerization.

Determination of Transfer Constant C_{Xa}. In the mechanism of Figure 2, both transfer steps C-1 and C-2 involve the addition of the radical to the C═S bond (kinetic constant k_{add} and k'_{add}), followed by the β fragmentation of the intermediate radical (kinetic constant k_β and k'_β)[3]. It is reasonable to assume that k_{add} is close to k'_{add}, k_β to k'_β, k'_β to k'-$_{add}$, and k_β to k-$_{add}$. On the basis of these approximations, the transfer constant for xanthate C_{Xa} can be written as eq 6:

$$C_{Xa} = \frac{k_{add}}{2k_p} \tag{6}$$

We have determined experimentally this transfer constant C_{Xa} of PBA and PDEGA radicals to the xanthate Rhodixan A1 via the O'Brien method[29] using eq 7:

$$\log\left(\frac{[Xa]}{[Xa]_0}\right) = C_{Xa} \log\left(\frac{[M]}{[M]_0}\right) \tag{7}$$

where [Xa] and [M] are the concentrations of unreacted xanthate and monomers at a certain time during the reaction, and $[Xa]_0$ and $[M]_0$ are the initial concentrations of xanthate and monomer. The ratios $[Xa]/[Xa]_0$ are reported vs $[M]/[M]_0$ in log−log scale in Figure 4. The dependence appears to be linear, as expected

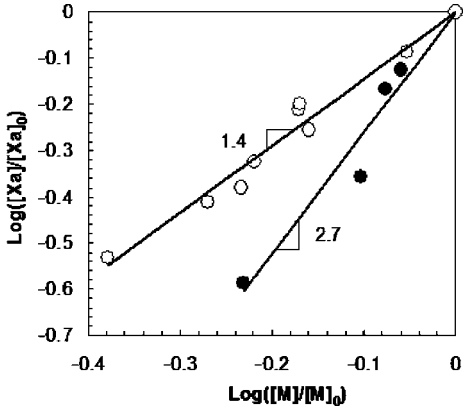

Figure 4. Conversion of butyl acrylate BA (●) and di(ethylene glycol) ethyl ether acrylate DEGA (○) monomers vs the conversion of xanthate measured by HPLC in a log−log plot for reaction proportions [DEGA]/[Xa]/[I] = [53]/[1]/[0.1] and [BA]/[Xa]/[I] = [73]/[1]/[0.1].

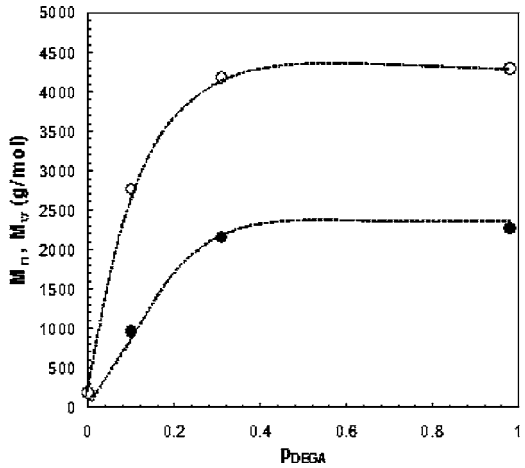

Figure 5. Variation of molar mass M_n (●) and M_w (○) of homomopolymer poly(di(ethylene glycol) ethyl ether acrylate) *h*-PDEGA chains measured by GPC vs conversion of monomers p for reaction proportion [DEGA]/[Xa]/[I] = [16]/[1]/[0.1]

from eq 7. From the slopes, we determined the transfer constants values C_{Xa} for PBA and PDEGA radicals to xanthate of respectively 2.7 and 1.4.

Evolution of M_n and M_w with Progress of the Reaction. Figure 5 presents the evolution of the molar masses M_n and M_w vs the conversion of monomers. It is clear that M_n and M_w do not increase linearly with the conversion of monomers. It is possible to calculate the evolution of the number-average degree of polymerization $\langle n\rangle$ vs the advancement of the reaction based on an ideally controlled mechanism. The number-average degree of polymerization $\langle n\rangle$ of a product can be written as eq 8:

$$\langle n\rangle = \frac{\sum_i i[P_i]}{\sum_i [P_i]} = \frac{\sum_i i[P_i^\bullet] + \sum_i i[P_i^{\otimes}] + \sum_i i[P_iX_a]}{\sum_i [P_i^\bullet] + \sum_i [P_i^{\otimes}] + \sum_i [P_iX_a]} \quad (8)$$

where $[P_i^\bullet]$, $[P_i^{\otimes}]$, $[P_iXa]$ represent the concentrations of chains made of i monomers, that, respectively, are bearing a radical, are dead, and are end-capped with a xanthate. $[P_i]$ is the sum of all these concentrations.

The upper part in eq 7 is the total concentration of consumed monomers and is thus equal to $[M]_0 - [M]$. It is thus easier to separate each term by writing the inverse of $\langle n\rangle$ as in eq 9:

$$\frac{1}{\langle n\rangle} = \frac{\sum_i [P_i^\bullet] + \sum_i [P_i^{\otimes}] + \sum_i [P_iX_a]}{[M]_0 - [M]} \quad (9)$$

The first two terms in the upper part of eq 9 correspond to the quantity of initiator consumed. This quantity is obviously smaller than the total amount of initiator introduced in the reactor, which is in turn 10 times smaller than the amount of xanthate. These two terms can be neglected as compared to the amount of Xa end-capped chains. Equation 9 can then be transformed into

$$\frac{1}{\langle n\rangle} = \frac{\sum_i [P_iX_a]}{[M]_0 - [M]} \quad (10)$$

The upper part of the right-hand side in eq 10 is the amount of xanthate that has reacted with a chain, i.e., $[Xa]_0 - [Xa]$, and the lower part is the amount of monomers that have reacted to form a chain, i.e., $[M]_0 - [M]$. Considering reactions C-1 and P, the consumption rates of xanthate and monomer follow eqs 11 and 12:

$$-\frac{d[Xa]}{dt} = \frac{1}{2} k_{add} \sum_i [P_i^\bullet][Xa] \quad (11)$$

$$-\frac{d[M]}{dt} = k_p \sum_i [P_i^\bullet][M] \quad (12)$$

After integration of the ratio between eq 11 and eq 12, one can write eq 13

$$[Xa] = [Xa]_0 \left(\frac{[M]}{[M]_0}\right)^{C_{Xa}} = [Xa]_0 (1-p)^{C_{Xa}} \quad (13)$$

where p is the conversion, defined as

$$p = \frac{[M]_0 - [M]}{[M]_0} \quad (14)$$

Notice that eq 13 is the relation used in the O'Brien method (eq 7). The final expression of the index of polymerization $\langle n\rangle$ in CRP is then given by eq 15:

$$\langle n\rangle = \frac{[M]_0}{[Xa]_0} \frac{p}{1-(1-p)^{C_{Xa}}} \quad (15)$$

Equation 15 was used in Figure 6 to plot the theoretical variations of M_n vs conversion p. If one looks at the bold curves of Figure 6 that neglect the effects of side-reactions, several behaviors can be differentiated:

•For C_{Xa} higher than 10, xanthate agent is consumed in the early stage of the reaction (step C-1) and the exchange of xanthate end groups is fast between the dormant and the growing chains (step C-2). Statistically, all the chains at any time during the reaction have experienced the same total period of growth. All chains have the same length and this length increases linearly with conversion of monomer p.

•For C_{Xa} close to 1, propagation and transfer rates are equal. Statistically speaking, a radical polymerizes until its degree of polymerization reaches [M]/[Xa]. Then, it reacts with a xanthate

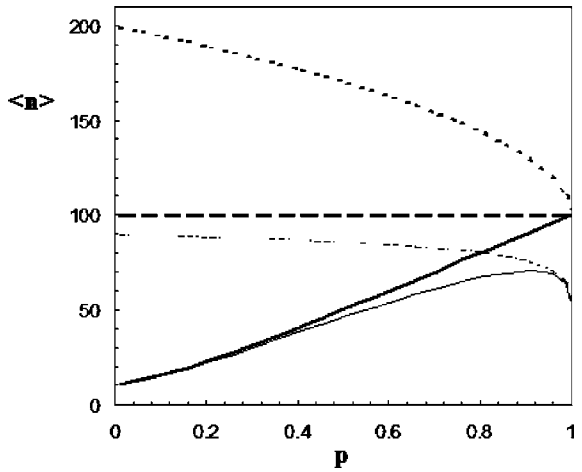

Figure 6. Degree of polymerization $\langle n \rangle$ of growing chains vs conversion of monomer p, as calculated for different values of C_{Xa} equal to 10 (—), 1 (— —), and 0.5 (- - -) with a ratio of monomer to xanthate equal to 100. Bold lines correspond to calculation without transfer to solvent ($C_s = 0$) based on eq 15 and thin lines correspond to calculation with transfer to solvent ($C_s = 10^{-3}$) based on eq 19.

Table 1. GPC Results for the Various Polymerization of Ba Monomers, with Different Ratios $M_t \approx M_{BA}$[BA]/[Xa][a]

$\langle n \rangle$	M_t (g/mol)	M_n (g/mol)	M_w (g/mol)	I_p
8	1000	1090	1534	1.41
23	3000	2984	4545	1.52
31	4000	2951	5263	1.78
93	12 000	6219	14 167	2.28
156	20 000	7621	19 844	2.60
234	30 000	8415	25 334	3.01

[a] All syntheses were done at 40% solid in EtOH ([BA] = 3.51 mol/L), at 70 °C with [I] = [Xa]/10.

Table 2. GPC Results for Various Polymerizations of Dega Monomers, with Different Ratios $\langle n \rangle \approx$ [DEGA]/[Xa][a]

$\langle n \rangle$	M_t (g/mol)	M_n (g/mol)	M_w (g/mol)	I_p
5	1000	1180	1900	1.61
16	3000	2433	4964	2.04
32	6000	4520	9312	2.06
53	10 000	6677	15 491	2.32
64	12 000	7118	17 011	2.39
80	15 000	7837	19 123	2.44
128	24 000	10 788	30 422	2.82
160	30 000	11 475	35 571	3.10

[a] All syntheses were done at 40% solids in EtOH ([DEGA] = 1.85 mol/L), at 70 °C with [I] = [Xa]/10.

(step C-1) and is definitely stabilized. Almost no exchange of xanthate end groups occurs (step C-2). The molar mass of the chains is independent of the conversion p.

•For C_{Xa} lower than 1, the reaction is not controlled any more.

The molar mass dependence with conversion presented in Figure 5 show a nonlinear dependence. This is roughly consistent with a low value of C_{Xa} but more data points would be needed for a precise comparison.

Evolution of M_n and M_w with Targeted Mass M_t: Evidence of Side-Reactions. Polymers of *h*-PBA and *h*-PDEGA with targeted M_t values between 1000 and 30 000 g/mol (1K and 30K) have been synthesized and analyzed by GPC (Tables 1 and 2). Figure 7 reports the final M_n and M_w values vs the targeted molar mass value M_t defined by eq 1. For M_t below 5000 g/mol, M_n is close to M_t as expected from eq 15. Above 5000 g/mol, M_n is always smaller than M_t and reaches a plateau at a value of 10 000 g/mol. This discrepancy with theory is a clear evidence that side-reactions cannot be neglected in the mechanism. One can note that M_w varies linearly with M_t in

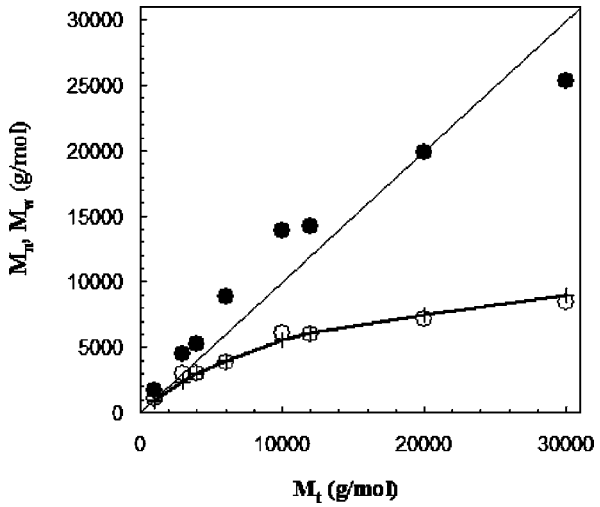

Figure 7. Variation of molar mass M_w (●) and M_n (○) of homopolymer poly(butyl acrylate) *h*-PBA chains measured by GPC vs targeted molar mass M_t. The symbols (+) and solid line (—) correspond to the adjustment of M_n data based on eq 19, using the experimental final conversion values p for each sample, and an adjusted value $C_s = 6 \times 10^{-4}$.

the whole range 0−30 000 g/mol. This suggests that side reactions produce mainly small chains. Possible side-reactions are transfer reaction of radicals to monomer, to polymer, to initiator or to solvent. Transfer of the radical to polymer tends to produce highly branched chains that are more compact than linear chains of the same mass. As seen by GPC measurements, where data are compared to linear standards, a highly branched chain would be interpreted as a linear chain of smaller mass. As a consequence, if branching of chains was the main side reaction phenomenon, the M_w values of the products would tend to decrease as compared to the targeted M_t values. Results of Figure 7 suggest the opposite conclusion. Another argument against transfer to polymer can be inferred from GPC results. The decrease of M_n relative to M_t means that the total number of chains is higher than expected, because the number of chains in a sample is inversely proportional to M_n.[30] Since the number of radicals is fixed and the number of chains increases, the transfer must occur to other species than the polymer itself in order to create more chains. Transfers to monomer, initiator, or solvent are then the only realistic transfer reactions to consider. In order to identify more clearly what side reaction occurs, an exact chemical composition of the products is necessary.

Analysis of Side-Products: ^{13}C NMR Results and Theoretical Estimation. On ^{13}C NMR spectra of *h*-PBA samples, the relative amount of quaternary carbons (peak at 48−50 ppm) was lower than 1% of all the carbons. This tends to confirm that intrachain transfer or backbiting of polymer chains are negligible. Unfortunately, the precision of the technique limits this analysis to polymers of masses lower than 3000 g/mol. The chains initiated by initiators I and the ones initiated by a leaving group R′ of the xanthate could also be identified. The integration of the peaks gave the expected molar proportion of 10/90. A large deviation from this ratio would have been a sign of an important side-reaction phenomenon. In the end, NMR data show that side reactions are negligible in the range of molar mass where NMR is sensitive to end groups, i.e., M_n lower than 3000 g/mol. This conclusion is consistent with results of Figure 7, where side reaction effects have been detected for M_t values larger than 5000 g/mol.

Quantitative Approach of Transfer to Solvent Effects. MALDI−TOF MS and NMR are limited to the analysis of short

chains, whereas the main effect of side reactions are observed for larger chains. Because of these analytical limitations, we have attempted a quantitative analysis taking transfer to solvent as the main side reaction. Several arguments permit us a priori to target transfer to solvent as the main side reaction. First, GPC evidence speaks against transfer to polymer. Second, the values for the transfer to solvent constant C_s of acrylate to ethanol at 70 °C are approximately 10^{-3}, which is fairly large.[31] And last, chain transfer to solvent has already proven to be a preponderant issue in RAFT processes.[6] Our starting hypothesis will be further supported as the appropriate arguments are developed.

Let us first tackle the effect of transfer to solvent on the M_n values. Transfer to solvent reactions (eq 16) occur in parallel to the propagation of the chains.

$$P_n^{\bullet} + S \xrightarrow{k_S} P_n^{\otimes} + S^{\bullet} \tag{16}$$

The rate of production of dead chain v_s is

$$v_s = \sum_i \frac{d[P_i^{\otimes}]}{dt} = \sum_i k_s[P_i^{\bullet}][S] \tag{17}$$

Combining eq 12 and eq 17, we can get an expression of the amount of dead chains produced by transfer to solvent vs p:

$$\sum_i [P_i^{\otimes}] = -\ln(1-p)C_s[S] \tag{18}$$

where $C_s = k_s/k_p$. Equation 18 can be inserted in eq 15 in order to take into account the effect of transfer to solvent. This leads to

$$\langle n \rangle = \frac{[M]_0 p}{[Xa]_0(1-(1-p)^{C_{Xa}}) - \ln(1-p)C_s[S]} \tag{19}$$

Equation 19 is plotted in Figure 6 to show the effects of transfer to solvent on the evolution of M_n vs conversion p. One can see a decrease of the average mass of chains in the sample at high conversion, a consequence of the production of new (and therefore necessarily shorter) chains. Also, one can notice in eq 19 that C_s is the only unknown parameter. C_s can therefore be determined by using eq 19 to adjust the experimental data of M_n vs M_t in Figure 7. For these adjustments, the experimental final values of p determined by HPLC were used for each sample. We finally obtained a C_s value of 6×10^{-4} for PBA. This value is consistent with transfer constant to solvent values found in the literature[31] for closely related systems. The transfer to solvent hypothesis therefore consistently explains the discrepancy of the measured molar mass vs the targeted molar mass. In order to avoid transfer to solvent issues in synthesis, one could lower the concentration of solvent, polymerize under bulk conditions, or use emulsion polymerization when monomer solubility allows for it. Polymerization in dilute solutions or bulk are however not realistic for industrial scale-ups. In the case of bulk polymerization, the number of transfer events to polymer and monomer would also increase. It is possible to stop the reaction before complete conversion and avoid transfer to solvent issues. However, since the excess of residual monomers and xanthate have to be removed, this procedure is also unrealistic for industrial scale-up.

For the present reactions in solution, the transfer to solvent implies that the number fraction of chains transferred to solvent will increase with the target molar mass. We intend now to determine quantitatively the weight fraction of dead chains.

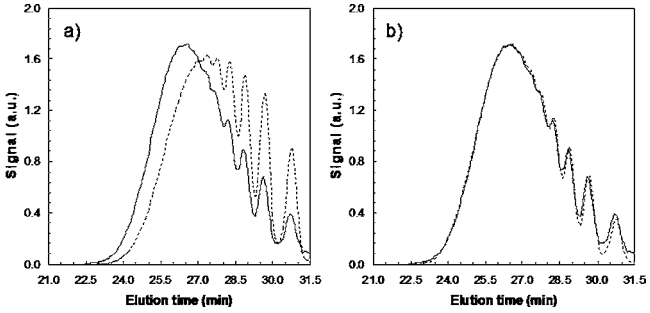

Figure 8. Functional analysis of homopolymer poly(butyl acrylate) *h*-PBA 1K: (a) GPC RI signal (—),and GPC UV signal (- - -); (b) GPC RI signal (—), GPC corrected UV signal, multiplied by a constant (- - -).

Functional Analysis: Quantification of Dead Chains. Double detection (refractive index (RI) and ultraviolet (UV) at 290 nm) GPC was used to get information on the polymer chains end groups. The refractive index signal S_{RI} is mostly sensitive to acrylate monomers. For a chain P_i of i monomers S_{RI} can be written as

$$S_{RI}(P_i) \propto i[P_i] \tag{20}$$

where $[P_i]$ is the concentration of all chains containing i monomers. The UV signal at 290 nm S_{UV} is sensitive to xanthate end groups only, not to acrylate groups. For a chain P_i of i monomers S_{UV} varies as

$$S_{UV}(P_i) \propto [P_i{-}Xa] \tag{21}$$

where $[P_i{-}Xa]$ is the concentration of −Xa end-capped chains containing i monomers. In order to compare RI and UV signals, the UV signal for a chain P_i was corrected according to

$$S^*_{UV}(P_i) = iS_{UV}(P_i) \tag{22}$$

This correction is only possible thanks to the calibration curve that associates a given polymer chain mass with a given elution time; practically, it is simply done by multiplying the UV signal at time t_i with the calibration mass for that time.

$$S^*_{UV}(t_i) = M(t_i)S_{UV}(t_i) \tag{23}$$

Parts a and b of Figure 8 show the GPC results for a *h*-PBA with a target molar mass of 1000 g/mol. Refractive index signal S_{RI} and raw UV signal S_{UV} are significantly different (Figure 8a). However, refractive index signal S_{RI} and corrected UV signal S^*_{UV}, multiplied by an adjustable constant, can be superimposed perfectly (Figure 8b). The determination of the adjustable constant absolute value requires a calibration between UV and RI signals with a sample of PBA chains whose amount of Xa end-capped chains is known. In absence of such sample, the adjustable constant between corrected UV and RI signals was chosen arbitrarily. Therefore, the fairly good superimposition of RI and corrected UV signals in Figure 8 does not mean that all chains are −Xa end-capped. It says that the fraction of −Xa end capped chains vs dead chains is independent of the chain length for *h*-PBA 1K. This result proved to be only true for very short chains, where effects of side reaction are not important. Let us now turn to longer chains. One could argue against the previous treatment of data that the UV signal correction is sensitive to the mass calibration of the GPC data. This limitation was avoided by comparing two samples of different targeted mass M_t without correction of UV data. The

Table 3. Relative Amounts of Dead Chains Per Sample between Two *h*-PBA Samples of Different Targeted Mass M_{t1} and M_{t2}

M_{t1}/M_{t2}	R_{exp}	R_{calc}
12K/4K	0.63	0.61
20K/12K	0.74	0.69
30K/20K	0.88	0.77

Table 4. Conversion p, Number Fraction X_n and Mass Fraction X_w of Dead *h*-PBA Chains in PBA Precursor Synthesis

$\langle n \rangle$	M_t (g/mol)	P	X_n	X_w
31	4000	0.990	0.29	0.17
93	12 000	0.983	0.49	0.40
156	20 000	0.982	0.62	0.59
234	30 000	0.977	0.69	0.68

RI and UV signals were recorded in the same conditions for the two samples. This insures that (i) the sensitivity of UV and RI detectors are the same for each sample, and (ii) the signals at a given time of elution t_i correspond to populations of the same mass for both samples. One can then calculate, for each time t_i, the ratio $r(t_i)$:

$$r(t_i) = \frac{(S_{RI}/S_{UV})_1}{(S_{RI}/S_{UV})_2} \tag{24}$$

where the indexes 1 and 2 refer to the two different samples. The results for three pairs of samples (12K/4K, 20K/12K, and 30K/20K), for which sample 1 has always a larger targeted mass than sample 2, lead to ratios $r(t_i)$ smaller than 1, for all pairs and for all elution times. This means that the relative amount of dead chains vs −Xa end-capped chains increases with the targeted mass. This is consistent with the fact that the larger polydispersities observed at higher targeted masses result from an increase of side reaction effects and from production of dead chains. We then integrated the $r(t_i)$ data for all t_i in order to estimate the relative average ratios of −Xa end capped chains between two samples. The experimental ratio R_{exp} values are reported in Table 3. These integrated values are smaller than one, because, qualitatively, the fraction −Xa end-capped chains decreases with M_t. Let us try to be more quantitative, and to compare these experimental R_{exp} values to theoretical calculations that take into account transfer to solvent issues. If other termination processes are neglected, the number fraction of dead chains resulting from transfer to solvent can be expressed as eq 25:

$$X_n(p) = \frac{\sum_i [P_i^{\otimes}]}{\sum_i [P_i^{\bullet}] + \sum_i [P_i^{\otimes}] + \sum_i [P_i\,Xa]} \tag{25}$$

After neglecting the concentration of active chains, we get eq 26:

$$X_n(p) = \frac{-\ln(1-p)C_s[S]}{[Xa]_0(1-(1-p)^{C_{Xa}}) - \ln(1-p)C_s[S]} \tag{26}$$

On the basis of eq 26 and using for all parameters their values determined experimentally, we have calculated the theoretical ratio R_{calc} of −Xa end-capped chains vs dead chains between two samples. The calculated values R_{calc} reported in Table 3 are quite comparable with experimental values R_{exp}. This result is a quantitative confirmation that transfer to solvent taken as the main side reaction allows a quantitative interpretation of the sample composition. After looking at the global fraction of dead chains in a sample, we then looked at the size distribution of dead chains and −Xa end-capped chains in a given sample. In an attempt to be as quantitative as possible, we developed a determination of the absolute fraction of −Xa end capped chains $\overline{R_{Xa}}$. In order to do so, we adjusted the prefactor to be applied to corrected UV signal so that the fraction of dead chains, integrated with this adjusted UV signal, matched the values X_n calculated from eq 26 (Table 4). We obtain by this method the absolute corrected UV signal, as compared to RI signal. The ratio $\overline{R_{Xa}}$ between this absolute corrected UV signal and the RI signal is now equal to the absolute fraction of −Xa end-capped chains and can be calculated for each chain size in a given sample. In Figure 9, the absolute ratio $\overline{R_{Xa}}$ is plotted vs the polymer molar mass for a PBA 12K sample. It appears that the fraction of −Xa end-capped chains is higher for larger chains, i.e., that the fraction of dead chains is higher for shorter chains. This is totally consistent with transfer to solvent events being the main source of dead chains. Indeed, these events are more probable toward the end of the reaction, when the solvent concentration is much larger than the monomer concentration. As a consequence, a larger proportion of dead chains are initiated toward the end of the reaction. As late starters, these chains eventually end up smaller than the average chains and with a smaller probability to exchange a xanthate. The absolute distribution of dead chains, also plotted in Figure 9, was then used to determine the absolute mass fraction of dead chain X_w. The results for X_w in several samples are presented in Table 4. These data will be useful in the next section for comparison with the amount of *h*-PBA chains present in diblock samples.

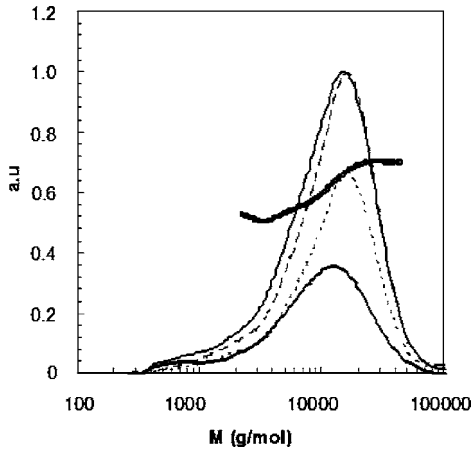

Figure 9. Functional analysis of homopolymer poly(butyl acrylate) *h*-PBA 12K, GPC RI signal (—) and corrected UV signal (- - -) normalized to their respective maximum value: (○) absolute fraction of −Xa end-capped chains $\overline{R_{Xa}}$; calculated distribution of −Xa end-capped chains (···) and of dead chains (—).

In the end, functional analysis has permitted a quantitative link between the amount of dead chains in a series of samples and a mechanism of transfer to solvent. It has also permitted a quantitative determination of the size distribution of dead chains in the samples.

B. Diblock copolymers PBA-*b*-PAA—Xa and PDEGA-*b*-PAA—Xa. GPC on the Diblock Copolymer. Figure 10 presents the GPC chromatograms of a *h*-PBA 4K precursor and the corresponding PBA-*b*-PAA 4K−20K diblock. The molar masses in Figure 10 are "polystyrene equivalent masses" since polystyrene standards were used for GPC calibration. We measured M_w and I_p values of 4500 g/mol and 1.5 for the precursor and 30 000 g/mol and 1.9 for the diblock. These values are consistent with the targeted values of molar mass (4K and

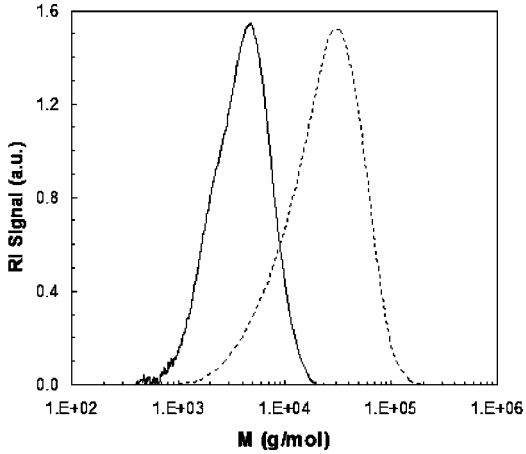

Figure 10. GPC chromatograms of homopolymer poly(butyl acrylate) *h*-PBA−Xa 4K precursor (solid line) and diblock copolymer poly(butyl acrylate)-*b*-poly(acrylic acid) PBA-*b*-PAA−Xa 4K−20K after methylation of PAA (dotted line).

Table 5. Analysis Results for Diblocks PBA-*b*-PAA[a]

	M_w (kDa)	I_p	X_{BA} (%)	X_{EA} (%)	X_{h-BA} (%)	X_{h-AA} (%)	X^*_{h-BA} (%)
3K−4K	13.4	1.51	0.13	0.09	0.15	0.25	0.35
3K−12K	15.7	1.64	0.12	0.04	0.06	0.49	0.30
4K−20K	30.0	1.91	0.12	0.01	0.04	0.30	0.24
6K−24K			0.11	0.04	0.09	0.51	0.45

[a] X_{BA} is the number fraction of monomer BA in the sample; X_{EA} is the number fraction of ethylated monomers in the sample; X_{h-BA} is the mass fraction of *h*-PBA in the sample; X_{h-AA} is the mass fraction of *h*-PAA in the sample. M_w is the "polystyrene equivalent molar mass" for the diblocks.

24K), and the expected values of I_p for CRP products (approximately 1.4). GPC results suggest that no major problem occurred during the two steps of the diblock synthesis. However, GPC is unable to give any detail on the exact composition of the product. At best, a closer look permits to see that the chromatogram of the diblock is asymmetric. This suggests that a portion of small chains are present in excess in the sample. But one cannot infer from GPC if this asymmetry comes from a fraction of diblocks of smaller molar mass, from dead chains of *h*-PBA that have not added a second block or from a fraction of *h*-PAA chains. GPC results for other samples studied are reported in Table 5.

NMR: Ratio BA/AA and Esterification. NMR results for all PBA-*b*-PAA samples studied are reported in Table 5. Figure 11 presents the ^{13}C NMR spectrum of the same PBA-*b*-PAA−Xa 4K−20K sample with all peaks associations made. We could identify the presence of three different monomers, butyl acrylate (BA), acrylic acid (AA) and ethyl acrylate (EA). BA and AA are the main ingredients of the reaction, whereas EA results from (trans)-esterification of BA or AA monomers by reaction with ethanol. ^{13}C NMR allows the determination of the fraction of acrylic acid and butyl acrylate groups that have reacted with the ethanol. Integration of the total carbonyl function (170−180 ppm) is set to 1, so that the fraction in number of esterified function X_{EA} can be estimated by integration of the carbon of ethyl acrylate peak at 60 ppm. The fraction of butyl acrylate X_{BA} is determined by integration of the carbon peaks at 18, 30, or 64 ppm. In Figure 11, 1% of monomers have been esterified by the solvent. More generally, we have been able to control this fraction below 5% for all syntheses, provided that the reaction was not run at high-temperature (70 °C) for too long, and that the polymers are not stored in ethanol for several months (even in a refrigerator at 6 °C). It was also preferable

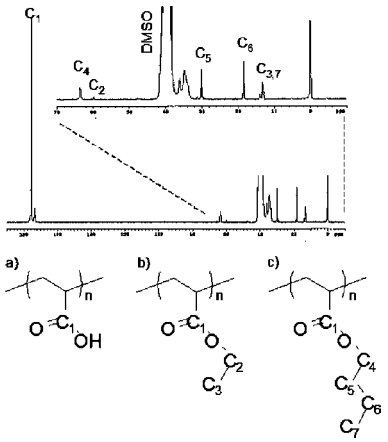

Figure 11. ^{13}C NMR spectrum of a diblock copolymer poly(butyl acrylate)-*b*-poly(acrylic acid) PBA-*b*-PAA−Xa 4K−20K with peaks labeled by the carbon number of developed chemical structures of (a) acrylic acid (AA), (b) ethyl acrylate (EA), and (c) butyl acrylate (BA).

to start the reaction by the PBA block, given that starting with the PAA block provides an acidic environment for the whole synthesis time, thus increasing the total esterification. Note that the control of low esterification levels in samples is very important for applications of the products. Indeed, ethyl acrylate moieties in the PAA block act as hydrophobic stickers between PAA chains in aqueous solutions[32] and aggregates of micelles in aqueous solution have been observed.[33] The esterification problem could have been totally avoided by using a solvent other than an alcohol.[6] However, we are aware that ethanol has its own advantages, namely its value in industrial scale-up. For the case of PDEGA-*b*-PAA samples, the rate of esterification could not be determined because the signal of EA and DEGA were overlapping. The optimized conditions for limited esterification established with PBA-*b*-PAA were therefore useful on the development of the synthesis of PDEGA-*b*-PAA.

^{13}C NMR was also used to determine the ratio between BA and AA. Regarding the example in Figure 11, we found a mass ratio of 0.24 which is close to the targeted ratio of 4K/20K = 0.2. Of course, the main limitation here is that NMR does not distinguish between PBA and PAA groups present either in homopolymer chains or in diblock chains. Mass ratio of the two block for PDEGA-*b*-PAA was also systematically checked by NMR and was always close to the expected value.

Amount of *h*-PBA: Quantitative LC-PEAT. An example of LC-PEAT separation for a PBA-*b*-PAA 6K−24K sample is presented in Figure 12. the homopolymer PBA eluted at 3 min, whereas diblocks and homopolymer *h*-PAA eluted together at 1.6 min.

We report in Table 5 the experimental mass fractions X_{h-BA} of homopolymer *h*-PBA in a sample, as determined by LC-PEAT. Results for all PBA-*b*-PAA samples studied are reported in Table 5. We then tried to determine the origin of the homopolymer *h*-PBA chains in diblock samples. The butyl acrylate BA in a diblock sample belongs either to *h*-PBA homopolymer chains or to PBA-*b*-PAA diblock chains. We can calculate the fraction X^*_{h-BA} of butyl acrylate BA belonging to *h*-PBA chains in the total amount of BA using eq 27:

$$X_{h-BA}{}^{*} = X_{h-BA}\left(1 + \frac{1}{X_{BA/AA}}\right) \qquad (27)$$

It is worth remarking that all butyl acrylate BA of a diblock sample comes from butyl acrylate BA of the precursor, given that all monomers are consumed before the second block is

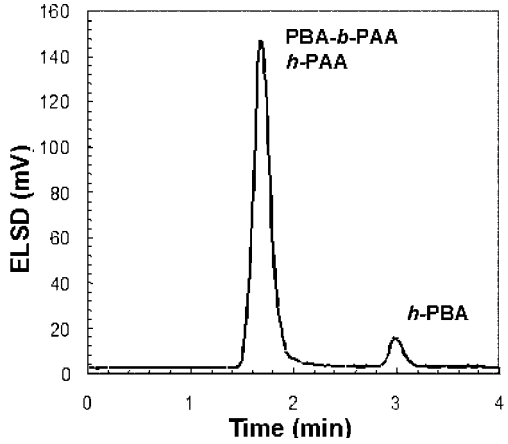

Figure 12. LC−PEAT chromatogram of a diblock copolymer poly(butyl acrylate)-*b*-poly(acrylic acid) PBA-*b*-PAA 6K−24K sample.

started. If all the precursor chains end-capped with a Xanthate had grown a block of PAA, the chains of *h*-PBA in a diblock sample would arise from (and only from) the dead chains in the precursor samples. In other words, the fraction of BA homopolymer X^*_{h-BA} in the diblock (Table 5) would match the fraction of BA dead chains X_w in the precursor (Table 4). It appears nevertheless that X^*_{h-BA} is always larger than X_w. This means that, in diblock samples, the *h*-PBA chains arise partially from the population of dead precursor chains, which cannot grow a second block. There is also another part of *h*-PBA chains in diblock samples corresponding to −Xa end-capped precursor chains that have not grown a second block, although they could have.

We also applied the same LC−PEAT procedure to PDEGA-*b*-PAA samples. As expected, the critical conditions adapted from PBA were not perfect for PDEGA. Nevertheless, using the same experimental conditions, the separation of homopolymer PDEGA from the rest of the sample was good enough to get well separated peaks. Quantitative measurements of homopolymer *h*-PDEGA amounts were achieved using aliquots of the first precursors *h*-PDEGA. We obtained contents of *h*-PDEGA lower than 10 wt %.

We then attempted to perform LC-PEAT experiments in critical conditions for *h*-PAA. LC-PEAT on PAA requires the use of normal phase columns. Their conditioning was difficult to achieve and led to non reproducible results. We therefore turned to capillary electrophoresis experiments for the determination of *h*-PAA amounts.

Amount of *h*-PAA: Quantitative CE. The amount of *h*-PAA in the samples was experimentally determined by capillary electrophoresis. Figure 13 presents the electropherogram of a PBA-*b*-PAA sample.

These results looked very similar to the ones on PVAc−PAA samples measured by Morel et al.[34] Using the same approach as Morel et al.,[34] we could attribute peaks 2 and 3 to the diblock, whereas peak 1 corresponded to homopolymer *h*-PAA.[33] Peak 2 corresponded to free unimers of diblocks and peak 3 corresponded to associated micelles of diblock.[33] The quantification of *h*-PAA was achieved by calibrating the integration value of peak 1 vs known added amounts of *h*-PAA. On the example of Figure 13, we determined a mass fraction of *h*-PAA of 25 wt % in the final diblock sample. We remarked that a similar value was obtained by simply comparing the integration of the diblock peak and the *h*-PAA peak. The latter method, although not rigorous, was more convenient and was used for all other samples. Results for all PBA-*b*-PAA samples studied are reported in Table 3. The relatively high amount of *h*-PAA

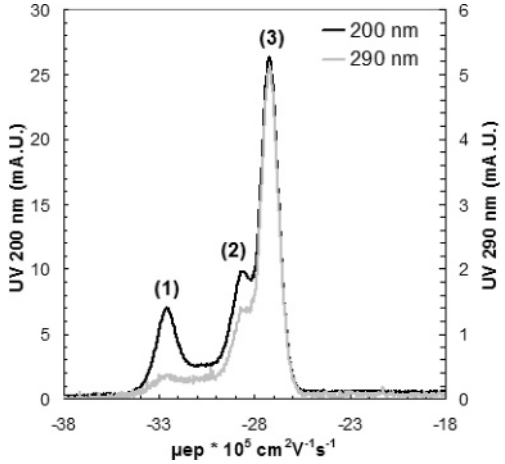

Figure 13. Capillary electrophoresis (CZE) electropherogram of a diblock copolymer poly(butyl acrylate)-*b*-poly(acrylic acid) PBA-*b*-PAA−Xa 4K−20K diblock as seen with UV detection at 200 (black line) and 290 nm (gray line).

has also been observed by Loiseau et al.[6] in conditions very similar to ours. In their case, transfer to solvent was invoked to explain this high amount of *h*-PAA. They had determined low values of the transfer constant *C* of their transfer agent to PAA (approximately one), and the transfer constant of PAA radical to ethanol (around 4.7×10^{-4}). The latter value was high enough to explain the large amount of *h*-PAA homopolymer in their final product (around 60 wt %). It is tempting to infer the same explanation for our system. To get further insight into the origin of *h*-PAA, we have compared the detection signals of CE at wavelengths of 200 and 290 nm. In Figure 13, an arbitrary prefactor was applied to the signal at 290 nm in order to have superimposed both UV signals at 200 nm and 290 nm for the diblock peaks (i.e., peaks 2 and 3). In comparison, the UV signals for the *h*-PAA peak (peak 1) do not superimpose at all. The signal at 290 nm is much lower than the signal at 200 nm. This means that the fraction of −Xa end capped xanthate is lower for *h*-PAA chains than for PBA-*b*-PAA chains, and/or that *h*-PAA chains have on average a higher degree of polymerization than PBA-*b*-PAA chains, which dilutes the relative content of xanthate. If transfer to solvent was the only distortion from ideal control, the mass fraction of −Xa end-capped chains would be very similar in the *h*-PAA and the PBA-*b*-PAA populations. Indeed, all along the reaction, the growing chains of these two populations have the same probability to transfer their radical to solvent and to exchange a xanthate. There is necessarily another parameter to take into account to explain the different xanthate ratio in the two populations. An important characteristic that we have overlooked up to now is the high rate of polymerization of PAA as compared that of PBA. In other words, assuming that the exchange constant k_{add} is similar for PBA and PAA, the transfer constant of xanthate C_{Xa} for the polymerization of PAA is lower than for the polymerization of PBA. In the beginning of the reaction, a consequent amount of long chains of *h*-PAA can grow in a non controlled way before the exchange of the control agent takes place (cf. Figure 6). These long chains of PAA induce lower apparent fraction of −Xa end capped chains than for average chains. Moreover, a small constant C_{Xa} implies that some chains will never exchange a xanthate during the synthesis. This latter effect was indeed observed as we have seen that a fraction of PBA−Xa precursor chains have not grown a second block. Since CE experiments are performed in aqueous solution, these PBA−Xa chains are trapped in the core of the diblock micelles and participate to the relative high ratio of Xa.

The same analysis by CE was also applied to PDEGA-*b*-PAA samples. As shown elsewhere,[33] the self-assembling of diblock chains into micelles in aqueous solution is much less pronounced for PDEGA-*b*-PAA than for PBA-*b*-PAA. There are almost no micelles of PDEGA-*b*-PAA in aqueous solution, just homopolymer *h*-PAA and free unimers of PDEGA-*b*-PAA. Still, the resolution of CE experiments was good enough to separate each population. The quantification of *h*-PAA was possible and again amounts of *h*-PAA around 30 wt % were found.

4. Conclusion

We have presented a thorough analytical study of diblock copolymer samples PBA-*b*-PAA (and PDEGA-*b*-PAA) synthesized by the CRP process MADIX. On the precursor samples, we have determined the transfer constant to xanthate C_{Xa} by the O'Brien method. C_{Xa} was found at 2.7 and 1.4 for respectively BA and DEGA. These values are too small to achieve very low polydispersities. However, they are large enough to ensure that most chains are terminated by a xanthate and can grow a second block. We then investigated the origin of side-reactions that were responsible for the higher polydispersity of large molar mass samples and the saturation of M_n values below 10 000 g/mol for the polymerization conditions used. We have demonstrated the presence of numerous dead chains by functional analysis. These dead chains were attributed to transfer to solvent events that occurred mainly at the end of the reaction. We could determine the transfer to solvent constant value $C_s \approx 6 \times 10^{-4}$. The amount of dead chains was then quantified, which has not sofar be shown in the literature to our best knowledge. We found a mass percentage of dead chains between 17 and 69 wt % for samples of targeted molar mass M_t between respectively 4000 and 30 000 g/mol. For the final diblock, conventional characterizations by GPC and NMR permitted only to check that chains had grown during the two steps of the reaction and that the final mass ratio of each block was correct. However, such characterizations were of little value for samples containing multiple side-products. We have quantified the amount of *h*-PBA (and *h*-PDEGA) in the diblock samples by LC−PEAT. These amounts of homopolymer of the first block were slightly higher than the amounts of dead chains produced in the precursor step. This means that PAA chains have not grown on all the precursor chains stabilized by a xanthate. We have then quantified the amount of *h*-PAA in the samples by capillary electrophoresis. Functional analysis showed that the *h*-PAA chains were less stabilized by xanthate than the diblock chains. This was attributed to high rate of polymerization of PAA relative to the transfer rate to xanthate. This high rate of polymerization could also explain that Xa end-capped precursor chains have not grown. Finally, the thorough quantitative analysis of CRP copolymers presented in this paper has proven highly valuable for in depth elucidation of the mechanism of a CRP process. It has allowed a precise chemical characterization of amphiphilic diblock copolymers samples. This is most valuable for the subsequent use and understanding of physical properties, such as self-assembling properties in aqueous solution and adsorption properties at hydrophobic interfaces, which are the subjects of future publications.

Acknowledgment. The authors acknowledge Rhodia, Inc. for the permission to publish this work, as well as for technical and financial support. They also want to thank Heiko Mauermann for performing NMR measurements, Douglas Radtke for help with GPC measurements, Patrick Dupuis for performing MALDI-TOF MS analysis and Mathias Destarac for interactive discussions on the MADIX process.

References and Notes

(1) Destarac, M.; Taton, D.; Zard, S. Z.; Saleh, T.; Six, Y. *ACS Symp. Ser.* **2003**, *854*, 536−550.
(2) Destarac, M.; Bzducha, W.; Taton, D.; Gauthier-Gillaizeau, I.; Zard, S. Z. *Macromol. Rapid Commun.* **2002**, *23*, 1049−1054.
(3) Adamy, M.; van Herk, A. M.; Destarac, M.; Monteiro, M. J. *Macromolecules* **2003**, *36*, 2293−2301.
(4) Farcet, C.; Belleney, J.; Charleux, B.; Pirri, R. *Macromolecules* **2002**, *35*, 4912−4918.
(5) Llauro, M.-F.; Loiseau, J.; Boisson, F.; Delome, F.; Lavadière, C.; Claverie, J. *J. Polym. Sci. Part A: Polym. Chem.* **2004**, *42*, 5439−5462.
(6) Loiseau, J.; Doërr, N.; Suau, J. M.; Egraz, J. B.; Llauro, M. F.; Lavadière, C.; Claverie, J. *Macromolecules* **2003**, *36*, 3066−3077.
(7) Copart, P.; Charmot, D.; Biadatti, T.; Zard, S.; Michelet, D. Patent WO 9858974, 1998.
(8) Copart, P.; Charmot, D.; Biadatti, T.; Zard, S.; Michelet, D. *Chem. Abstr.* **1999**, *130*, 82018.
(9) Chapon, P.; Mignaud, C.; Lizarraga, G.; Destarac, M. *Macromol. Rapid Commun.* **2003**, *24*, 87−91.
(10) Lefay, C.; Belleney, J.; Charleux, B.; Guerret, O.; Magnet, S. *Macromol. Rapid Commun.* **2004**, *25*, 1215−1220.
(11) Couvreur, L.; Lefay, C.; Belleney, J.; Charleux, B.; Guerret, O.; Magnet, S. *Macromolecules* **2003**, *36*, 8260−8267.
(12) Chong, Y. K.; Le, T. P. T.; Moad, G.; Rizzardo, E.; Thang, S. H. *Macromolecules* **1999**, *32*, 2071−2074.
(13) Gaillard, N.; Guyot, A.; Claverie, J. *J. Polym. Sci.: Part A: Polym. Chem.* **2003**, *41*, 684−698.
(14) Lavadière, C.; Dörr, N.; Claverie, J. P. *Macromolecules* **2001**, *34*, 5370−5372.
(15) Zard, S. Z. *Angew. Chem., Int. Ed. Engl.* **1997**, *36*, 672−685.
(16) Grubisic, Z.; Rempp, P.; Benoit, H. *J. Polym. Sci., Part B: Polym. Lett.* **1967**, *5*, 753−759.
(17) Beuermann, S.; Paquet, D. A.; McMinn, J. H.; Hutchinson, R. A. *Macromolecules* **1996**, *29*, 4206−4215.
(18) Gorshkov, A. V.; Much, H.; Becker, H.; Pasch, H.; Evreinov, V. V.; Entelis, S. G. *J. Chromatogr.* **1990**, *523*, 91−102.
(19) Zimina, T. M.; Kever, J. J.; Melenavskaya, E. Yu.; Fell, A. F. *J. Chromatogr.* **1992**, *593*, 233−241.
(20) Pasch, H.; Rode, K. *J. Chromatogr. A* **1995**, *699*, 21−29.
(21) Pasch, H.; Brinkmann, C.; Much, H.; Just, U. *J. Chromatogr.* **1992**, *623*, 315−322.
(22) Berek, D. *Macromolecules* **1998**, *31*, 8517−8521.
(23) Lee, H.; Lee, W.; Chang, T.; Choi, S.; Lee, D.; JI, H.; Nonidez, W. K.; Mays, J. W. *Macromolecules* **1999**, *32*, 4143−4146.
(24) Khaledi, M. G. *High Performance Capillary Electrophoresis: Theory, Techniques and Applications*; Khaledi, M. G., Ed.; John Wiley and Sons: New York, 1998.
(25) Stepanek, M.; Podhajecka, K.; Tesarova, E.; Prochazka, K.; Tuzar, Z.; Brown, W. *Langmuir* **2001**, *17*, 4240−4244.
(26) Gallardo, A.; Lemus, A. R.; Roman, J. S.; Cifuentes, A.; Diez-Maza, J. C. *Macromolecules* **1999**, *32*, 610−617.
(27) Aguilar, M. R.; Gallardo, A.; Roman, J. S.; Cifuentes, A. *Macromolecules* **2002**, *35*, 8315−8322.
(28) Morishima, Y. *Chin. J. Polym. Sci.* **2000**, *18*, 323−336.
(29) O'Brien, J. L.; Gornick, F. *J. Am. Chem. Soc.* **1955**, *77*, 4757−4763.
(30) In a sample of total mass M_T, and number average molar mass M_n, the total number of chains n_T (in moles) is equal to $n_T = M_T/M_n$.
(31) Masson, J. C. *Polymer Handbook*, 3rd ed.; Wiley: New York, 1989; Chapter II "polymerizations and depolymerization", p II-94. The transfer constant from butyl acrylate to ethanol is given at 4.28×10^{-4} at 80 °C.
(32) Grandjean, J.; Mourchid, A. *Phys. Rev. E* **2005**, *72*, 4, 041503. Grandjean, J.; Mourchid, A. *Europhys. Lett.* **2004**, *65*, 5, 712−718.
(33) Jacquin, M.; Futterer, T.; Talingting, R.; Berret, J. F.; Cottet, H.; Muller, P.; Théodoly, O. Chemical analysis and aqueous solution properties of PBA-*b*-PAA Charged Amphiphilic Block Copolymers synthesized by MADIX. Manuscript in preparation.
(34) Morel, A.; Cottet, H.; In, M.; Deroo, S.; Destarac, M. *Macromolecules* **2005**, *38*, 15, 6620−6628.